Direct Evidence of Cobalt Oxyhydroxide Formation on a La0.2Sr0.8CoO3 Perovskite Water Splitting Catalyst

Anthony Boucly
Paul Scherrer Institut https://orcid.org/0000-0003-1436-3462
Luca Artiglia (luca.artiglia@psi.ch)
Paul Scherrer Institute https://orcid.org/0000-0003-4683-6447
Emiliana Fabbri
Paul Scherrer Institut https://orcid.org/0000-0002-8627-6926
Dennis Palagin
Paul Scherrer Institut https://orcid.org/0000-0001-5251-3471
Dino Aergerter
Paul Scherrer Institut
Daniele Pergolesi
Paul Scherrer Institute https://orcid.org/0000-0002-6231-0237
Zbynek Novotny
Physik-Institut, Universität Zürich
Nicolo Comini
Physik-Institut, Universität Zürich
J. Trey Diulus
Physik-Institut, Universität Zürich
Thomas Huthwelker
Swiss Light Source, Paul Scherrer Institut
Markus Ammann
Paul Scherrer Institut, CH-5232 Villigen, Switzerland https://orcid.org/0000-0001-5922-9000
Thomas Schmidt
Electrochemistry Laboratory, Paul Scherrer Institute https://orcid.org/0000-0002-1636-367X

Article

Keywords: oxygen evolution reaction (OER), electrocatalysis, perovskite water splitting catalyst

DOI: https://doi.org/10.21203/rs.3.rs-289935/v1

Abstract

Understanding the mechanism of oxygen evolution reaction (OER) on perovskite materials is of great interest to tailor the synthesis of better catalyst materials. Despite the huge amount of literature reports, the complexity of catalytic systems and scarce in situ and operando surface sensitive spectroscopic tools render the detection of active sites and the understanding of the reaction mechanisms challenging. Here, we carried out and compared in situ and ex situ ambient pressure X-ray photoelectron spectroscopy experimental procedures on a $La_{0.2}Sr_{0.8}CoO_3$ perovskite OER catalyst. Experimental results show that segregated surface strontium, which is present in the as prepared sample, is leached into the electrolyte after immersion, leading to surface cobalt active sites enrichment. Such cobalt-enriched oxide surface evolves into a new phase, whose spectral feature is detected in situ, during/after OER. With the help of theoretical simulations, such species is assigned to cobalt oxyhydroxide, providing a direct evidence of its crucial role in the reaction.

Introduction

Hydrogen-based systems have the capability to be a viable solution to compensate the intermittent nature of renewable energy. In this scenario, when a surplus of renewable energy is available, water electrolyzers can convert it into hydrogen, which can be reused to produce electricity or fuels when needed. For this reason, great efforts have been recently dedicated to the understanding of water electrolysis and the improvement of catalytic materials towards the development of efficient and cost-effective water electrolyzers.[1] Particularly, the anodic reaction, i.e., the oxygen evolution reaction (OER), is affected by slow kinetics and high overpotential, reducing the efficiency of the whole device.[2] Thus, a widespread commercialization of water electrolyzers urges for the development of highly active, stable and cost-effective electrocatalysts.

Perovskite-type oxides are promising materials for OER in an alkaline environment. Such materials allow a broad variety of elemental compositions and, thus, fine-tuning of their properties.[3, 4, 5, 6] However, despite the large scientific interest, there is still no unequivocal consensus on the reaction mechanism occurring on the surface of perovskite oxides. The “conventional” mechanism is based on four concerted proton-electron transfer steps.[1, 2, 7, 8] Recently, a new oxygen evolution mechanism, called lattice oxygen evolution reaction (LOER), has been proposed. It involves the oxidation of perovskite lattice oxygen for the production of molecular oxygen.[2, 5, 6, 9, 10] In addition, both proposed reaction mechanisms seem to be often accompanied by catalyst surface reconstruction, leading to the loss of crystallinity and the development of a superficial oxyhydroxide phase.[5, 11, 12, 13, 14] Such a phase, dynamically assembled during the electrocatalytic reaction, is believed to be extremely active toward OER.[5, 6, 12, 13, 14, 15] Understanding of how/when such an oxyhydroxide phase forms, and what the main properties leading to high OER activity are, remain open questions of paramount importance. This calls for advances in surface sensitive *operando* and/or *in situ* characterizations.

Recent progresses in ambient pressure X-ray photoelectron spectroscopy (APXPS) allow the *in situ* surface investigation of OER catalysts. Particularly, by means of the “dip and pull” method, which makes use of a standard electrochemical three electrode setup, it is possible to simultaneously perform electrochemical and XPS characterizations.[16, 17, 18, 19] In the “dip and pull” method, a thin liquid electrolyte layer (10–30 nm thickness) is stabilized at the sample surface. This provides potential control of the working electrode while performing XPS measurements. However, in order to probe the buried interface of the electrode, it is necessary to generate photoelectrons with high kinetic energies, which can travel through the thin electrolyte layer and subsequent ambient of ~ 30 mbar. For this reason, tender X-rays (3000-10,000 eV) are typically used.[17, 20]

Under OER conditions, OH^- in the thin electrolyte layer are consumed as diffusion limitations from the bulk solution can lead to their depletion. This creates a high ohmic resistance that makes real *operando* measurements challenging. A second possibility for investigating catalyst surface changes induced by OER, is performing XPS measurements *ex situ* directly after electrochemical measurements. In this case, measurements are not performed while a potential is applied to the working electrode. The possibility to carry out electrochemical measurements in an XPS chamber while carefully controlling the reaction environment during the analysis can still allow for preserving and observing irreversible catalyst surface modifications induced by an applied potential. This *ex situ* approach overcomes drawbacks associated with the thin electrolyte meniscus, required for “dip and pull” measurements. Soft X-rays (hv < 2000 eV) can be utilized and their energy tuned to be sensitive to the topmost layers of the electrode, where active species form.

In the present study, we have compared the results obtained by *in situ* and *ex situ* APXPS measurements on $La_{0.2}Sr_{0.8}CoO_{3-\delta}$ (LSCO) thin film perovskite. LSCO is known to be an interesting, highly OER active perovskite.[5, 15] Depending on the preparation temperature, LSCO thin films can present different degrees of strontium segregation. Strontium-containing species segregated on the surface (hydroxides or carbonates) are soluble in water.[21] Thus, the immersion of LSCO electrodes in water leads to a removal of the strontium segregated layer, exposing more cobalt active sites for the OER. As a result, the most active OER catalyst is the one with the highest initial amount of strontium surface segregation.[21] In this work, the most OER active LSCO thin film[21] has been investigated by *in situ* and *ex situ* APXPS, showing not only the removal of superficial, segregated strontium upon contact with the liquid electrolyte, but also the formation of a completely new oxyhydroxide phase, as demonstrated by combining experimental results with theoretical simulations of the core electron binding energies. To our knowledge, this is the first direct spectroscopic observation of such surface-active species involved in OER, which were postulated in several research contributions.[5, 13, 14] Our results also highlight the possibility to get important information about the nature of active sites making use of *ex situ* investigations carried out under well controlled conditions.

Results

Figure 1 shows a sketch that summarizes the main measurements performed in the present study using APXPS *ex situ* and *in situ* and an electrochemical three electrode cell (WE: working electrode, CE: counter electrode, RE: reference electrode). The electrochemical protocol, carried out in the three electrode cell with the WE fully immersed in the electrolyte solution, consisted of a stepwise potential increase up to 1.65 V vs. RHE and then of 50 cyclic voltammograms (CVs) performed between 1 and 1.65 V vs. RHE at 100 mV/s. *Ex situ* measurements were carried out by pulling the WE completely out of the solution and using soft X-rays after rinsing in pure water. In this case, the electrolyte must be removed because low kinetic energy photoelectrons cannot be measured in a background pressure higher than 20 mbar. *In situ* measurements were carried out using tender X-rays and the so called the “dip and pull” method.[17, 18, 19, 20]
FIGURE 1: Schematics of the experiment. During the initial step, the sample fully dipped in the electrolyte and the electrochemical measurement are done. Once those measurements are done, in the case of the in situ experiment (tender X-rays) we pull the sample directly in the measurement position while holding the potential and proceed with XPS measurements probing through the thin electrolyte. In the case of the ex situ experiment (soft X-rays), we pull out the sample, put it in storage under a partial pressure of 26 mbar and remove the electrolyte beaker before reintroducing the sample and bringing it to XPS measurement position under a partial pressure of 1 mbar.

In this latter case, APXPS measurements could be performed under an applied potential with CE and RE fully immersed in the electrolyte and the WE partially immersed in the electrolyte with the upper part (measured spot) only covered by a thin layer of electrolyte able to maintain electrical contact. High kinetic energy photoelectrons generated by tender X-rays can be measured at background pressures higher than 20 mbar and contain information about the interface of the WE buried under the thin layer of electrolyte. The detailed experimental approach is described in the experimental methods. As shown in Fig. 1, LSCO increases its capacitive current (in the potential region between 1 and ~ 1.65 V vs. RHE) over the 50 cycles, while slightly decreasing its OER current (above ~ 1.65 V vs. RHE). This suggests that the sample surface undergoes some modifications during the CVs. To unveil such (electro)chemically driven surface modifications, the electrode has been investigated *in situ* and *ex situ* by means of APXPS.

As shown in Fig. 2a, initially the Sr 3d core level spectrum acquired *in situ* shows two features that can be deconvoluted in two doublets (spin orbit splitting of 1.8 eV and branching ratio of 1.5).[21] The first one, at a binding energy of 133.3 eV (Sr $3d_{5/2}$, orange color) corresponds to surface-segregated strontium species. The second one, centered at 131.5 eV (Sr $3d_{5/2}$, green color) is ascribed to bulk-like (lattice) strontium.[16, 22, 23] Using a higher photon excitation energy, a second core-level peak of strontium, Sr 2p, was acquired and is shown in Figure S2a. In this case, two components, corresponding to surface and bulk strontium, can be detected. Being the KEs of Sr 2p and Sr 3d in Figure S2a are approximately 3050 and 2160 eV (corresponding to 8.8 nm and 6.6 nm attenuation length), respectively, the former contains information from a larger depth. The relative intensity of the surface component in the case of Sr 2p ($Sr_{surf}/Sr_{Bulk=}0.27$) is lower than that calculated from Sr 3d (0.43), supporting the fact that such strontium compounds segregate at the surface. The Sr 3d photoemission signal acquired *ex situ*, shown in Figure S2b, was acquired with a KE of approximately 760 eV. This corresponds to 3 nm attenuation length and

allows focusing the analysis on segregated strontium, whose relative intensity is maximal ($Sr_{surf}/Sr_{Bulk=}2.45$) among all the spectra shown in Figure S2. Upon immersion of the sample in the electrolyte solution and application of a potential of 1.65 V vs RHE, the signal of Sr 2p acquired *in situ* (Figure S2a) displays a clear evolution. A single peak (light green color), centered at 1938.8 eV, is present. The same line shape evolution is detected *ex situ* with soft X-rays (Figure S2b): a single doublet (Sr $3d_{5/2}$ at 133.0 eV, light green) is used to fit the spectrum collected after electrochemical measurements. It is important to highlight that the binding energy of the new doublet matches neither that of surface nor that of bulk strontium. This means that the electronic state of strontium is modified during CV cycles. The presence of a single component both under bulk (Sr 2p, Figure S2a) and surface (Sr 3d, Figure S2b) sensitive conditions suggests the formation of a new strontium-containing phase, promoted by the interaction with the electrolyte and OER cycles. Most likely, the local coordination environment of strontium changes after the reaction, and its binding energy is slightly affected. In addition, Fig. 2a and 2b show that, after electrochemistry, the intensity of Sr 3d decreases in a relevant way, whereas that of cobalt (Co 2p core-level peak) increases. This indicates that immersion of the electrode in the electrolyte solution followed by CV measurements leads to leaching of the segregated strontium layer, modification of its local structure, and cobalt enrichment at the surface.

FIGURE 3: O 1s XPS spectra from the *in situ* experiment (a) and the *ex situ* experiment (b) with red, purple and black curves corresponding to the “As prepared”, “Under 1.65 V vs RHE/ After 1.65 V vs RHE” and “After Electrochemistry” states, respectively. The green, orange, red, light blue and dark blue components correspond to the perovskite bulk, surface, hydroxyls, water gas phase and electrolyte signal, respectively.

The evolution of the Sr 3d/Co 2p ratio (corrected by photon flux and photo-ionization cross sections), evaluated both during *in situ* and *ex situ* measurements, is reported in Fig. 2b and Table S3. After introduction in the analysis chamber (“As prepared”), the electrode shows a ratio of 3.95 and 3.54, measured *in situ* and *ex situ*, respectively. After EC, such values decrease to 0.75 and 0.77. In both experiment the system ends up with more cobalt exposed at the surface, in fair agreement with previous observations.[21] The fact that the Sr/Co ratios acquired *in situ* and *ex situ* show similar values (within the error), suggests that strontium leaching takes place within the probing depth of *in situ* measurements. Co 2p photoemission peaks are shown in Fig. 2a, and display the line shape of Co(III) in the lattice of perovskites (Co $2p_{3/2}$ centered at approximately 780 eV).[24, 25, 26, 27] When looking for chemical changes on the cobalt due to EC, a slight modification of the line shape is observed between the “As prepared” and “After EC” conditions (see also Figure S3a) with a more pronounced bump in the satellite structure present at a binding energy around 785–790 eV while the main peak at 780 eV remains unchanged. This possibly indicates a slight evolution of the surface. However, this change is too small to speculate on the nature of such modification. *Ex situ* experiments (Figure S3b and S3c), have been used to cross check the *in situ* results. Both the Co 2p and Co $L_{2,3}$ edges show negligible line shape modifications, suggesting that negligible changes of the electronic state of cobalt take place within the probed depth, which is 2.2 nm and 2.8 nm for Co 2p and Co $L_{2,3}$, respectively.

Figure 3 displays the comparison between O 1s measurements performed *in situ* (Fig. 3a) and *ex situ* (Fig. 3b). The signal of oxygen is of particular importance because it contains information about lattice components (oxygen in the lattice of LSCO surface termination) and surface species that are present or form during reaction. O 1s spectra of the “as prepared” sample were separated into two components. The first one, at a binding energy of 528.9 eV, corresponds to oxygen in the perovskite lattice, as commonly reported in the literature.[22, 28, 29] The second component, at a binding energy of 531.5 eV, is assigned to oxygen in the termination layer.[28] *In situ* measurements (Fig. 3a) were performed with two excitation energies (2300 and 5000 eV), in order to vary the information depth within the same measurement. The relative intensity of the 531.5 eV component shows an increasing trend passing from 5000 to 2300 eV, and becomes the main component of O 1s acquired *ex situ* (Fig. 3b). This proves that oxygen in the termination layer has a thickness distribution comparable/limited to the probing depth of *ex situ* measurements (2.2 nm). *In situ* measurements performed during EC show a complex line shape due to the presence of a thin liquid layer on top of the WE. As reported in Fig. 3a, the peak at 532.6 eV corresponds to condensed water and that at 535.0 eV to water vapor in equilibrium with the liquid (background in the analysis chamber). Liquid water is not present during *ex situ* measurements (Fig. 3b), because spectra were acquired at a 1 mbar water vapor background, without a stabilized electrolyte layer on top of the electrode and no potential applied. Two further components, centered at 529.0 eV and 530.6 eV, were used to deconvolute O 1s acquired *in situ* during EC. While the former (green color) is still assigned to oxygen in the lattice of LSCO, the latter (red color) reflects the presence of new oxygen-containing species, different from those in the termination layer observed after sample introduction. Interestingly, the O 1s spectrum acquired *ex situ* shows only this new component, at a binding energy of 531.0 eV. Once again, we want to stress that O 1s acquired *ex situ* has a KE of approximately 480 eV, whereas the KE *in situ* is 4460 eV. This corresponds to a relevant change of the probed depth from 2.2 nm to 6 nm, and demonstrates that newly formed species are located at the surface. We tentatively attribute the new component to hydroxyls, which form at the surface of the sample during electrochemistry.

Measurements performed after EC give other interesting information about the evolution of the sample surface. Photoemission peaks can be separated into three components, assigned to oxygen in the lattice of LSCO (529.0 eV, green color), surface hydroxyl groups (530.6 eV) and oxygen in the termination layer of LSCO (531.6 eV), which are detected in both measurement conditions. The reappearance of oxygen in the termination layer of LSCO suggests that hydroxyls may originate from such species during OER while part of them converts back under UHV conditions. It is generally assumed that for LSCO perovskites, cobalt is the active site for OER.[2, 30] Experimental data described above suggest the formation of hydroxyls during reaction, while the surface is enriched in cobalt. Therefore, the formation of a cobalt oxyhydroxide phase during reaction can be speculated. Such species are well visible in the O 1s spectrum,

but not in the Co 2p. Based on the literature, line shape modifications of Co 2p upon formation of hydroxide are extremely small and mostly affect the structure of shake-up satellites.[31, 32]

To further support our hypothesis, theoretical simulations of the core electron binding energies of different oxygen species on LSCO have been performed and compared with the experimental data.

FIGURE 4: Oxygen binding energy simulation results compared to the measured results. Colored binding energy values correspond to the calculated data, with green being the bulk perovskite oxygen (O2-), orange being the surface signal corresponding to adsorbed carbonate species on the strontium segregated layer, and red being the hydroxyls groups formed during electrochemistry.

Figure 4 shows the spectrum of O1s acquired *ex situ* after EC measurements, deconvoluted using the same peak components described above. The core electron binding energy value calculated for a bulk LSCO structure (Fig. 4, right) oscillates between 528.8 and 529.0 eV (O atoms computationally split in two groups, depending on their location with respect to La and Sr, see Figure S4 in SI), in good agreement with the position of the green component detected experimentally (528.9–529.0 eV). The structure of strontium carbonate was used to simulate oxygen in the termination layer of LSCO (strontium segregations soluble in water, Fig. 4, left), which should correspond to the highest BE peak (orange color in the O 1s). Simulations estimate a binding energy value between 531.6 and 531.9, in fair agreement with the experimental value of 531.5 eV. A series of possible defects that could form on cobalt oxide-terminated LSCO during EC have been simulated adsorbing hydroxyl groups on the CoO_2 topmost layer. Three possible structures are presented in Fig. 4 (top) and correspond to different configurations of the adsorbed hydroxyl. These structures represent some of the possible geometrical structures of the surface hydroxyl groups, and correspond to the following situations: a) formation of the surface OH^- group in the place of a surface oxygen defect; b) adsorption of the OH^- group on the CoO_2-terminated surface; and c) formation of multiple OH^- groups in the place of multiple surface oxygen defects. Whereas these three structures by no means represent a comprehensive set of possible surface structures (some additional structures are presented in Figures S5 and S6 in SI), they provide sufficient variability to check whether they may in principle correspond to the observed experimental data. The simulated binding energy of OH^- in the three structures varies in the 530.2531.0 eV range. The centroid of the new O 1s peak component detected experimentally is at 530.6 eV (red color), at the center of the simulated BE range. Most likely, a collection of different hydroxyl species form on top of the electrode during EC, thus the experimental peak is a convolution of different species displaying similar BE values. In summary, an excellent agreement between the experiment and theory is found, and theory supports the hypothesis of cobalt oxyhydroxide active phase formation during reaction

Discussion

A perovskite LSCO catalyst for the OER has been fully characterized by means of APXPS *in situ*, probing the buried solid-liquid interface with tender x-rays, and *ex situ*, carrying out surface-sensitive measurements with soft x-rays in a controlled water vapor background after reaction. Different experimental approaches provide complementary information that allow a complete characterization of the surface during and after OER. Immersion of LSCO in the electrolyte solution leads to the leaching of

surface segregated strontium species, leaving cobalt active sites exposed. Thanks to *in situ* and *ex situ* photoemission of the O 1s performed during and after OER, respectively, a new phase has been detected and assigned to surface cobalt oxyhydroxide. Such results have been confirmed by means of theoretical calculations of core electron binding energies.

The direct observation of perovskite surface reconstruction during OER, and the clear detection of a spectroscopic signature, undoubtedly indicates that the real active site for the perovskite OER activity is a Co-based oxyhydroxide layer. However, the perovskite structure is still visible underneath Co oxyhydroxide, suggesting an equilibrium between the two within the present experimental conditions. This represents a step forward toward the investigation of active site combining *in situ* and ex situ surface sensitive measurements. In particular, the *ex situ* experimental protocol can be easily reproduced in several facilities and avoids well known drawbacks connected to the use of the “dip and pull” method. Theoretical calculations of the core electron binding energy are a powerful tool to facilitate the interpretation of complex spectroscopic data. The first spectroscopic experimental proof of cobalt oxyhydroxide formation represents an advancement in the understanding of the reaction mechanism of OER on perovskite materials and will have relevant implications for future works concerning this topic.

Methods

Materials preparation.

$La_{0.2}Sr_{0.8}CoO_{3-\delta}$ (LSCO) thin film samples were prepared by Pulsed Laser Deposition (PLD) using a KrF excimer laser (Lambda Physik LPX 300, 25 ns pulses, λ = 248 nm) with a laser fluence at the target surface set at ~ 1.25 J/cm^2 and a frequency of 10 Hz. The films were grown using a background pressure of 0.1 mbar of O_2 for 30 min. The distance between the target and the substrate was fixed at 4 cm. A platinum paste spot was painted next to the substrate to monitor the temperature with a pyrometer. The samples were prepared on Al_2O_3(001) substrates (Crystek) at a temperature of 550°C. After deposition, the samples were annealed in an oxygen-saturated atmosphere for 30 min at 350°C. Figure S1 shows a representative XRD plot of one of our films in comparison with that of the LSCO powders. The diffraction peak of the Al_2O_3 substrate is marked with an asterisk. It can be seen that the film is polycrystalline but textured, along the (110) and (111) out-of-plane orientation.

To ensure good electrical conductivity, a gold frame (150 nm) with a titanium sticking layer (8 nm) was deposited by sputtering along the perimeter of the substrate on top of the films. The sample was fixed at the bottom of a 5x1 cm² glass lamella using a double face copper tape. The electrical connection with the manipulator was made through a gold wire.

XPS characterization.

A sketch of the experimental protocols employed to investigate LSCO *in situ* and *ex situ* by means of APXPS is shown in Fig. 1. Tender X-ray APXPS experiments (hereafter called *in situ*) were carried out at

the PHOENIX I beamline of the Swiss Light Source Synchrotron (SLS), making use of the solid liquid interface endstation.[19] The sample was first analyzed under ultra-high vacuum (UHV) conditions at different excitation energies: 2300 eV and 5000 eV (hereafter referred as “As prepared”). The estimated inelastic mean free path (IMFP) by using the QUASES-IMFP-TPP2M program[33] at hv = 2300 eV and hv = 5000 eV are for O1s 2.8 nm (KE = 1760 eV) and 6 nm (KE = 4460 eV), for Co 2p 2.5 nm (KE = 1510 eV) and 5.7 nm (KE = 4210 eV), for Sr 3d 3.3 nm (KE = 2160 eV) and 6.4 nm (KE = 4860 eV) and for Sr 2p 4.4 nm (KE = 3060 eV, only at hv = 5000 eV). Considering our setup geometry, around 90% of the XPS signal comes within 2λ giving a probing depth for those energies of 5.6 and 12 nm for O 1s, 5 nm and 11.4 nm for Co 2p, 6.6 nm and 12.8 nm and 8.8 nm for Sr 2p (only at hv = 5000 eV). The sample was then dipped in a 0.1 M KOH beaker and the potential was increased stepwise to reach 1.65 V vs RHE. 50 cyclic voltammograms (CVs) were performed at 100 mV/s, ending the protocol at 1.65 V vs RHE. While the potential was held at 1.65 V vs RHE, the LSCO thin film was slowly pulled out from the electrolyte until a thin electrolyte meniscus was stably formed allowing electrical connection between LSCO, the counter electrode (CE), and reference electrode (RE) via the electrolyte solution. In this configuration, the sample surface is investigated (called “Under 1.65V”) by tender X-ray APXPS at hv = 5000 eV, through the electrolyte meniscus still covering the sample surface and ensuring potential control (*in situ* characterization). Afterwards, the sample was fully dipped into the KOH beaker and the potential brought back to open circuit voltage (OCV). The sample was then cleaned in ultra-pure water before being characterized under UHV at hv = 2300 eV to have its final state (called “After EC”) in the most surface sensitive condition available.

Soft X-ray APXPS experiments (hereafter called *ex situ*) were carried out at the In Situ Spectroscopy beamline (X07DB) of SLS, making use of the same endstation mentioned above.[19] Like in tender X-ray experiments, the sample was first analyzed under UHV conditions at two different photoelectron kinetic energies (KEs): 480 eV and 780 eV. For those kinetic energies, the estimated inelastic mean free paths are 1.1 nm and 1.5 nm giving a probing depth of 2.2 and 3 nm for 480 eV and 780 eV, respectively. At each probed depth, Sr 3d, La 4d, O 1s and either Co 2p (at KE ≈ 480 eV) or Co 3p (at KE ≈ 780 eV) core level spectra were acquired. Two different core level peaks of cobalt were used due to the limit in maximum excitation energy available at the beamline. Once the initial UHV characterization was performed (hereafter named “As prepared”), the sample was dipped in a beaker containing 0.1 M KOH. After 50 CVs (ending at 1.65 V vs. RHE), the potential was held at 1.65 V vs. RHE while the sample was completely removed from the electrolyte solution (no longer under potential control). Prior to APXPS measurements, the sample was dipped into an ultra-pure water beaker to rinse the KOH present at the sample surface. The sample was then brought into storage, both KOH beaker and ultra-pure beaker are taken out and the sample reintroduced into the analysis chamber. Finally, the LSCO surface was characterized by APXPS under a water partial pressure of 1 mbar (hereafter named “After 1.65 V”). After characterization, the sample was brought back once again into storage and both KOH and ultra-pure water beaker reintroduced. Then the sample was also reintroduced and dipped into the KOH to end the electrochemical protocol (bringing the potential back to OCV). Using the same method described above, we removed the beaker and characterized the sample in UHV to have its final state (hereafter named “After EC”). The

difference between the first and last CV cycle, showing the appearance of the Co redox couple is shown in Fig. 1.

For both tender and soft X-ray APXPS experiments, photoemission spectra were normalized to the photon flux and to the total ionization cross-section. The C 1s peak centroid was used as a reference, with its binding energy fixed at 284.8 eV. All peaks were fitted with Gaussian functions after subtraction of a Shirley background. Deconvolution fitting parameters are shown in Table S1 and Table S2 for soft and tender X-ray experiments, respectively.

Simulation of the core-electron binding energy

All theoretical calculations in this work have been performed with the all-electron full-potential DFT code FHI-aims[34, 35] within the periodic boundary conditions model. Geometry optimizations of periodic models were carried out using the standard generalized gradient approximation with the PBE functional[36] and the "tier2" atom-centered basis set using "tight" settings for numerical integrations. For the subsequent binding energy calculations, electronic exchange and correlation was treated on the hybrid functional level with the PBE0 functional.[37]

For all considered models, La/Sr ratio is assumed to be 1/3 to minimize the required unit cell size, with the resulting perovskite composition corresponding to $La_{0.25}Sr_{0.75}CoO_3$ for the bulk systems and $La_{0.25}Sr_{0.75}CoO_{2.5}$ for the surface-terminated systems. All initial geometries correspond to a cubic unit cell. During the geometry optimization the symmetry was allowed to relax freely.

In order to follow the changes in the nature of the surface species, the electron binding energy of O 1s electrons uses standard definitions of ionization energies from the respective core levels.[38] These calculations are carried out at a hybrid functional level for the fully periodic structural models. We have shown recently that this methodology yields reliable results that can be compared to experimental X-ray photoelectron spectroscopy.[39, 40]

Declarations

Competing interests

The authors declare non competing interest

Authors Contributions

The manuscript was written through contributions of all authors. / All authors have given approval to the final version of the manuscript.

Acknowledgements

The post-doc position of AB is funded by the Energy and Environment division of the Paul Scherrer Institute. ZN, NC and JTD: Swiss National Science Foundation, project grant 200020_172641. JTD additionally acknowledges the funding from European Union's Horizon 2020 program (FP-RESOMUS – MSCA 801459)

References

1. Fabbri E, Habereder A, Waltar K, Kotz R, Schmidt TJ. Developments and perspectives of oxide-based catalysts for the oxygen evolution reaction. *Catal Sci Technol* **4**, 3800–3821 (2014).
2. Fabbri E, Schmidt TJ. Oxygen Evolution Reaction-The Enigma in Water Electrolysis. *Acs Catal* **8**, 9765–9774 (2018).
3. Grimaud A, *et al.* Activating lattice oxygen redox reactions in metal oxides to catalyse oxygen evolution. *Nature Chemistry* **9**, 457 (2017).
4. Pan Y, *et al.* Direct evidence of boosted oxygen evolution over perovskite by enhanced lattice oxygen participation. *Nature Communications* **11**, 2002 (2020).
5. Fabbri E, *et al.* Dynamic surface self-reconstruction is the key of highly active perovskite nano-electrocatalysts for water splitting. *Nature Materials* **16**, 925–931 (2017).
6. Beall CE, Fabbri E, Schmidt TJ. Perovskite Oxide Based Electrodes for the Oxygen Reduction and Evolution Reactions: The Underlying Mechanism. *Acs Catal*, (2021).
7. Rossmeisl J, Logadottir A, Nørskov JK. Electrolysis of water on (oxidized) metal surfaces. *Chemical Physics* **319**, 178–184 (2005).
8. Man IC, *et al.* Universality in Oxygen Evolution Electrocatalysis on Oxide Surfaces. *ChemCatChem* **3**, 1159–1165 (2011).
9. Yoo JS, Rong X, Liu Y, Kolpak AM. Role of Lattice Oxygen Participation in Understanding Trends in the Oxygen Evolution Reaction on Perovskites. *Acs Catal* **8**, 4628–4636 (2018).
10. Yoo JS, Liu Y, Rong X, Kolpak AM. Electronic Origin and Kinetic Feasibility of the Lattice Oxygen Participation During the Oxygen Evolution Reaction on Perovskites. *The Journal of Physical Chemistry Letters* **9**, 1473–1479 (2018).
11. Binninger T, *et al.* Thermodynamic explanation of the universal correlation between oxygen evolution activity and corrosion of oxide catalysts. *Scientific Reports* **5**, 12167 (2015).
12. Chung DY, *et al.* Dynamic stability of active sites in hydr(oxy)oxides for the oxygen evolution reaction. *Nature Energy* **5**, 222–230 (2020).
13. Lopes PP, *et al.* Dynamically Stable Active Sites from Surface Evolution of Perovskite Materials during the Oxygen Evolution Reaction. *Journal of the American Chemical Society*, (2021).
14. Baeumer C, *et al.* Tuning electrochemically driven surface transformation in atomically flat LaNiO3 thin films for enhanced water electrolysis. *Nature Materials*, (2021).
15. Kim BJ, *et al.* Functional Role of Fe-Doping in Co-Based Perovskite Oxide Catalysts for Oxygen Evolution Reaction. *Journal of the American Chemical Society* **141**, 5231–5240 (2019).

16. Stoerzinger KA, *et al.* Speciation and Electronic Structure of La1 – xSrxCoO3 – δ During Oxygen Electrolysis. *Topics in Catalysis* **61**, 2161–2174 (2018).
17. Axnanda S, *et al.* Using "Tender" X-ray Ambient Pressure X-Ray Photoelectron Spectroscopy as A Direct Probe of Solid-Liquid Interface. *Scientific reports* **5**, 9788 (2015).
18. Ali-Löytty H, *et al.* Ambient-Pressure XPS Study of a Ni-Fe Electrocatalyst for the Oxygen Evolution Reaction. *Journal of Physical Chemistry C* **120**, 2247–2253 (2016).
19. Novotny Z, *et al.* Probing the solid-liquid interface with tender x rays: A new ambient-pressure x-ray photoelectron spectroscopy endstation at the Swiss Light Source. *Rev Sci Instrum* **91**, 023103 (2020).
20. Favaro M, Abdi F, Crumlin E, Liu Z, van de Krol R, Starr D. Interface Science Using Ambient Pressure Hard X-ray Photoelectron Spectroscopy. *Surfaces* **2**, 78–99 (2019).
21. Boucly A, *et al.* Surface Segregation Acts as Surface Engineering for the Oxygen Evolution Reaction on Perovskite Oxides in Alkaline Media. *Chemistry of Materials* **32**, 5256–5263 (2020).
22. Crumlin EJ, *et al.* In Situ Ambient Pressure X-ray Photoelectron Spectroscopy of Cobalt Perovskite Surfaces under Cathodic Polarization at High Temperatures. *The Journal of Physical Chemistry C* **117**, 16087–16094 (2013).
23. Crumlin EJ, *et al.* Surface strontium enrichment on highly active perovskites for oxygen electrocatalysis in solid oxide fuel cells. *Energy & Environmental Science* **5**, 6081 (2012).
24. Yang J, *et al.* Oxygen Vacancy Promoted O2 Activation over Perovskite Oxide for Low-Temperature CO Oxidation. *Acs Catal* **9**, 9751–9763 (2019).
25. Seim H, Nieminen M, Niinistö L, Fjellvåg H, Johansson L-S. Growth of LaCoO3 thin films from β-diketonate precursors. *Applied Surface Science* **112**, 243–250 (1997).
26. Armelao L, Bettinelli M, Bottaro G, Barreca D, Tondello E. LaCoO3 Nanopowders by XPS. *Surface Science Spectra* **8**, 24–31 (2001).
27. Álvarez-Serrano I, *et al.* Magnetic behaviour governed by Co spin transitions in LaCo1 – xTixO3(0 â©½xâ©½ 0.5) perovskite oxides. *Journal of Physics D: Applied Physics* **41**, 195001 (2008).
28. Stoerzinger KA, *et al.* Reactivity of Perovskites with Water: Role of Hydroxylation in Wetting and Implications for Oxygen Electrocatalysis. *The Journal of Physical Chemistry C* **119**, 18504–18512 (2015).
29. van der Heide PAW. Systematic x-ray photoelectron spectroscopic study of La1-xSrx-based perovskite-type oxides. *Surface and Interface Analysis* **33**, 414–425 (2002).
30. Badruzzaman A, Yuda A, Ashok A, Kumar A. Recent advances in cobalt based heterogeneous catalysts for oxygen evolution reaction. *Inorganica Chimica Acta* **511**, (2020).
31. Kudielka A, Schmid M, Klein BP, Pietzonka C, Gottfried JM, Harbrecht B. Nanocrystalline cobalt hydroxide oxide: Synthesis and characterization with SQUID, XPS, and NEXAFS. *Journal of Alloys and Compounds* **824**, 153925 (2020).

32. Yang J, Liu H, Martens WN, Frost RL. Synthesis and Characterization of Cobalt Hydroxide, Cobalt Oxyhydroxide, and Cobalt Oxide Nanodiscs. *The Journal of Physical Chemistry C* **114**, 111–119 (2010).
33. Tougaard S. QUASES-IMFP-TPP2M code for the calculation of the inelastic electron mean free path, Version 3.0.).
34. Blum V, *et al.* Ab initio molecular simulations with numeric atom-centered orbitals. *Computer Physics Communications* **180**, 2175–2196 (2009).
35. Ren X, *et al.* Resolution-of-identity approach to Hartree–Fock, hybrid density functionals, RPA, MP2 andGWwith numeric atom-centered orbital basis functions. *New Journal of Physics* **14**, (2012).
36. Perdew JP, Burke K, Ernzerhof M. Generalized Gradient Approximation Made Simple. *Physical Review Letters* **77**, 3865–3868 (1996).
37. Adamo C, Barone V. Toward reliable density functional methods without adjustable parameters: The PBE0 model. *The Journal of Chemical Physics* **110**, 6158–6170 (1999).
38. Tardio S, Cumpson PJ. Practical estimation of XPS binding energies using widely available quantum chemistry software. *Surface and Interface Analysis* **50**, 5–12 (2018).
39. Artiglia L, Sushkevich VL, Palagin D, Knorpp AJ, Roy K, van Bokhoven JA. In Situ X-ray Photoelectron Spectroscopy Detects Multiple Active Sites Involved in the Selective Anaerobic Oxidation of Methane in Copper-Exchanged Zeolites. *Acs Catal* **9**, 6728–6737 (2019).
40. Palagin D, Sushkevich VL, van Bokhoven JA. Water Molecules Facilitate Hydrogen Release in Anaerobic Oxidation of Methane to Methanol over Cu/Mordenite. *Acs Catal* **9**, 10365–10374 (2019).

Figures

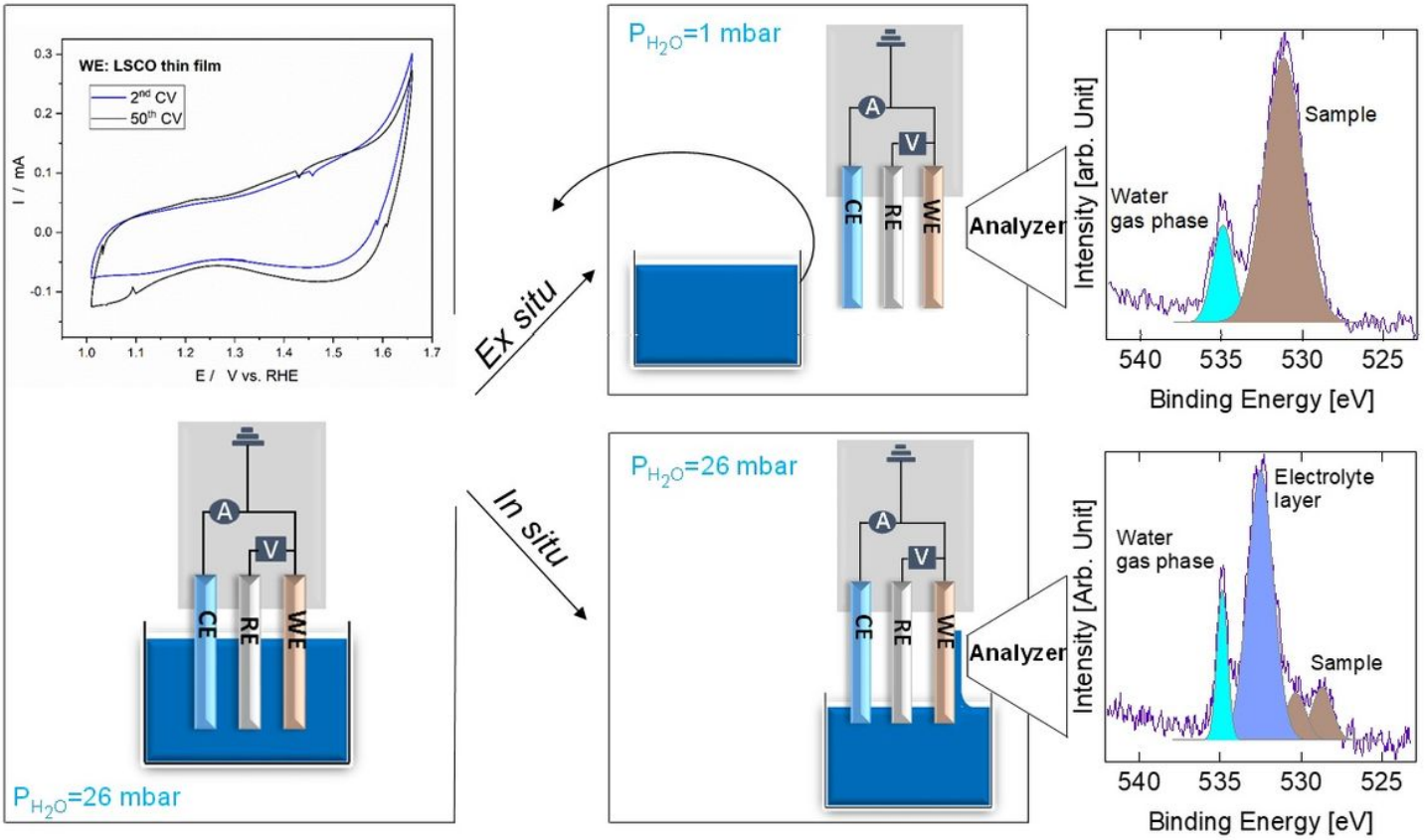

Figure 1

Schematics of the experiment. During the initial step, the sample fully dipped in the electrolyte and the electrochemical measurement are done. Once those measurements are done, in the case of the in situ experiment (tender X-rays) we pull the sample directly in the measurement position while holding the potential and proceed with XPS measurements probing through the thin electrolyte. In the case of the ex situ experiment (soft X-rays), we pull out the sample, put it in storage under a partial pressure of 26 mbar and remove the electrolyte beaker before reintroducing the sample and bringing it to XPS measurement position under a partial pressure of 1 mbar.

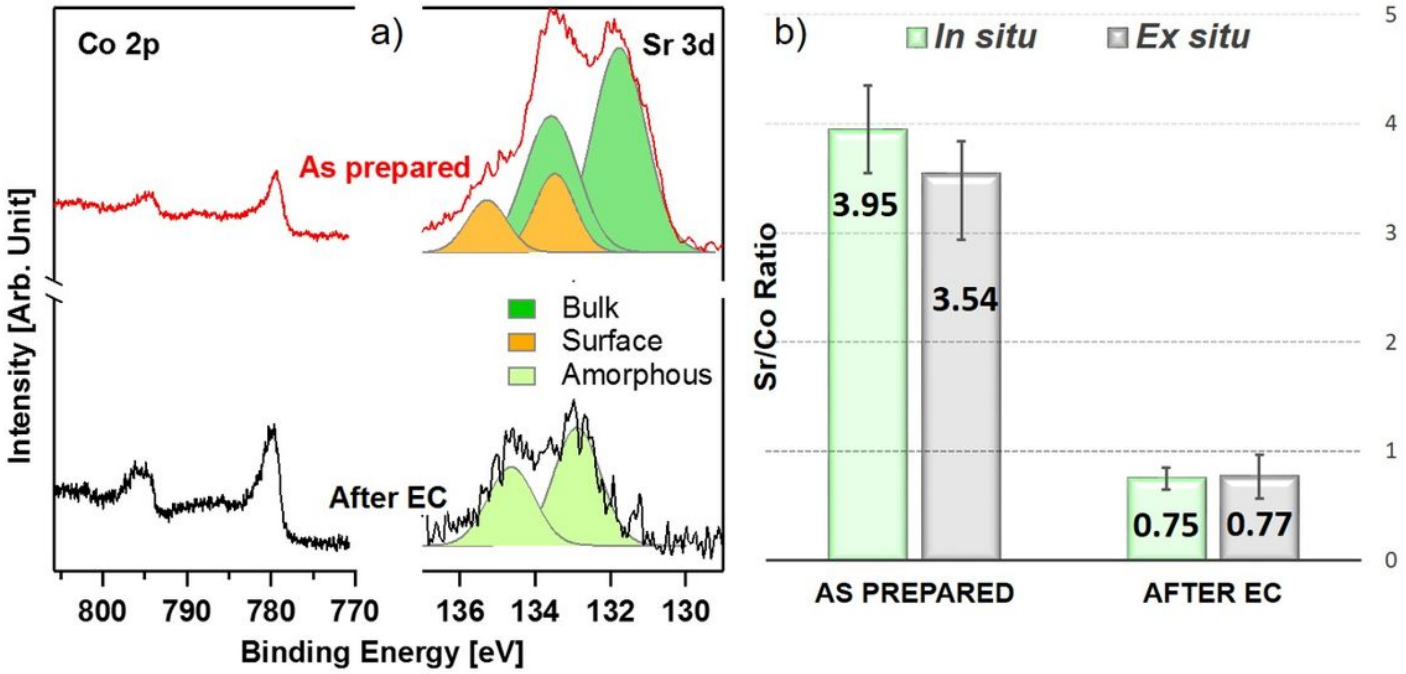

Figure 2

Photoemission spectra(a) acquired at hv = 2300 eV during the in situ experiment showing the collapse of the Sr 3d signal peak (right) compared to the Co 2p signal (left) with red and black curves corresponding to the “As prepared” and “After Electrochemistry” state, respectively. The dark green component of the strontium deconvolution corresponds to the bulk signal, orange corresponds to the surface signal, and the light green single component seen after electrochemistry corresponds to the new single species displaying a shift in binding energy. The Co/Sr ratios calculated from those spectra are shown as histogram (b) with the in situ experiment plotted in light green and the ex situ one plotted in gray

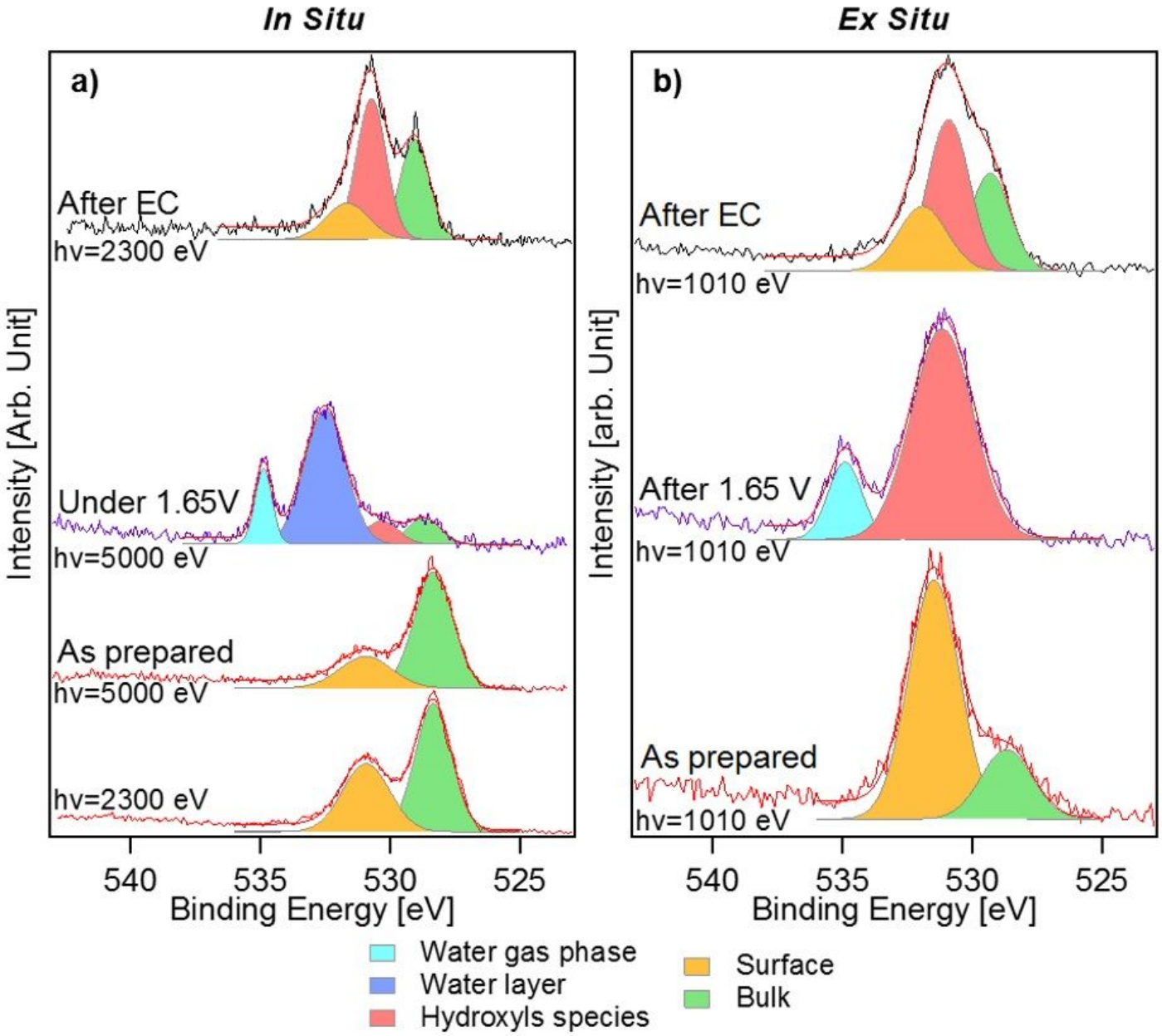

Figure 3

O 1s XPS spectra from the in situ experiment (a) and the ex situ experiment (b) with red, purple and black curves corresponding to the “As prepared”, “Under 1.65 V vs RHE/ After 1.65 V vs RHE” and “After Electrochemistry” states, respectively. The green, orange, red, light blue and dark blue components correspond to the perovskite bulk, surface, hydroxyls, water gas phase and electrolyte signal, respectively.

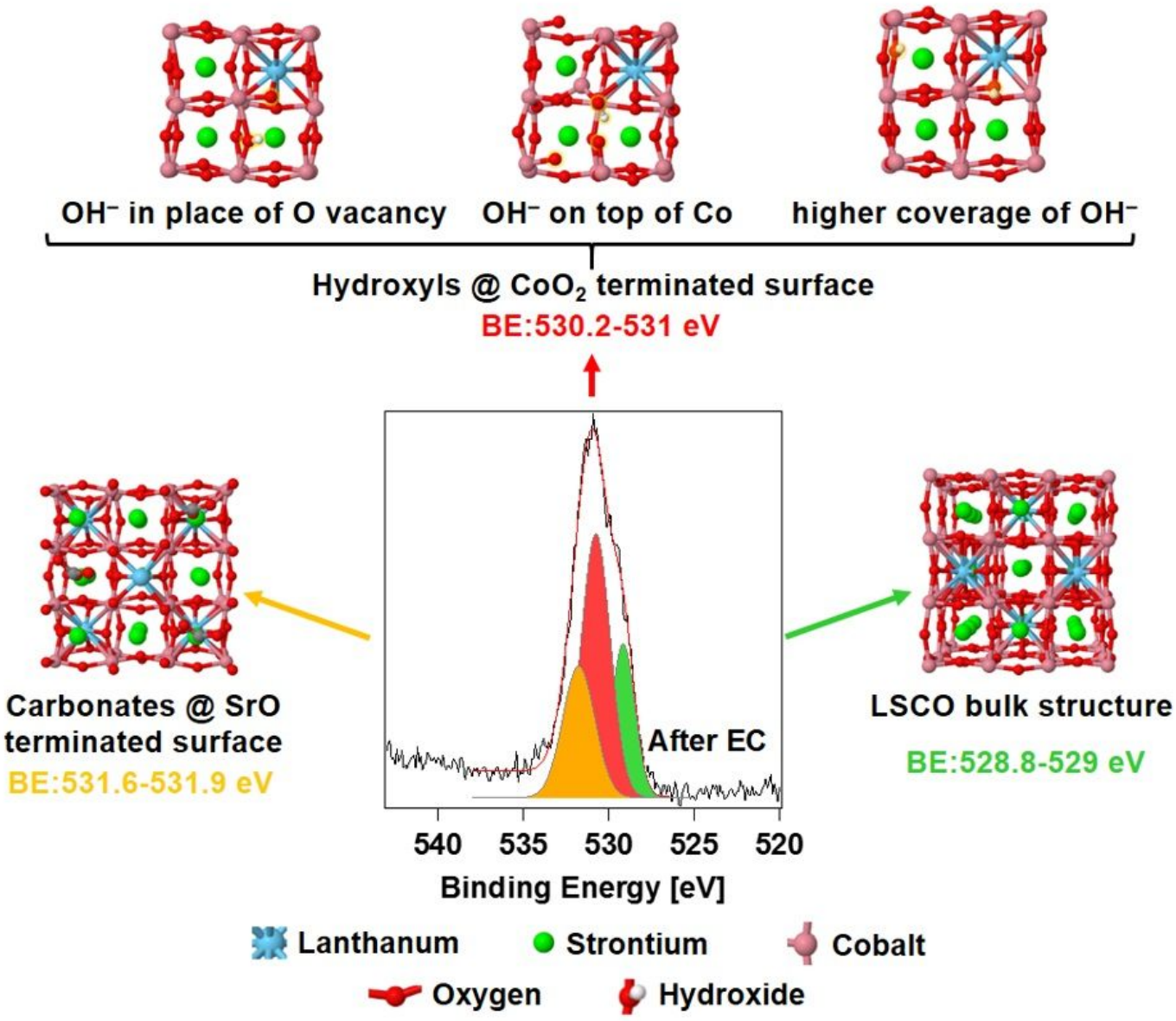

Figure 4

Oxygen binding energy simulation results compared to the measured results. Colored binding energy values correspond to the calculated data, with green being the bulk perovskite oxygen (O2-), orange being the surface signal corresponding to adsorbed carbonate species on the strontium segregated layer, and red being the hydroxyls groups formed during electrochemistry.